Microporous and Mesoporous Materials 152 (2012) 253–261

Contents lists available at SciVerse ScienceDirect

Microporous and Mesoporous Materials

journal homepage: www.elsevier.com/locate/micromeso

Cr(VI) sorption by using clinoptilolite and bacteria loaded clinoptilolite rich mineral

Beyhan Cansever Erdoğan *, Semra Ülkü

Chemical Engineering Department, Faculty of Engineering, Izmir Institute of Technology, Gulbahce Koyu, 35430 Urla, Izmir, Turkey

ARTICLE INFO

Article history:
Received 2 May 2011
Received in revised form 4 October 2011
Accepted 3 November 2011
Available online 23 November 2011

Keywords:
Cr(VI) sorption
Bacteria loaded clinoptilolite rich mineral
Characterization
Kinetic model

ABSTRACT

Batch sorption experiments were performed in order to understand the potential value of local clinoptilolite rich mineral and its bacteria loaded form in Cr(VI) sorption. The results indicated that Cr(VI) sorption capacities of the sorbents were increased after bacteria loading and the clinoptilolite rich mineral is a promising material in Cr(VI) sorption. Zeta potential and Fourier Transform IR (FTIR) analysis were performed to explain the possible mechanism involved in the Cr(VI) sorption. The results revealed that non-electrostatic forces played a significant role rather than the electrostatic forces. The existence of non-electrostatic forces was confirmed by the FTIR results.

1. Introduction

Chromium (Cr), one of the most important pollutants, exists in the effluents of various industries such as leather tanning, electroplating, pigments and metal finishing. Although it has oxidation states of +2, +3, +4, +5 and +6, only two states, trivalent and hexavalent chromium, are stable in the environment [1]. Chromium(VI), which is more toxic than Cr(III), is found in anionic form and it is soluble in aqueous phase almost within the entire pH range. It causes lung cancer, gastrointestinal disorders, dermatitis and kidney damage in humans. In addition it is toxic to other organisms [2,3]. Reduction, precipitation, nano-ultrafiltration and membrane technologies are among the waste treatment methods applied for chromium(VI) removal. But due to the concerns related to high energy input and large amounts of secondary wastes produced, further research on alternative methods is needed. In recent years, investigation on sorption with natural, synthetic and biological sorbents has gained much attention. The cost of the technology and the availability, the removal efficiency and the cost of the sorbent are the prime factors to be considered in the selection of the sorbent. The usage of clinoptilolite rich mineral has special value due to its low cost and abundancy in nature. Clinoptilolite rich mineral is a crystalline hydrated aluminosilicate. The framework structure is made up of AlO_4 and SiO_4 tetrahedra and three types of channels (A, B and C). Water and exchangeable cations such as magnesium, sodium, calcium and potassium also exist in its structure. It has high potential for separation, purification, adsorption and ion exchange depending on the type of exchangeable cations and their specific positions within the framework structure [4–12]. Additionally, high selective cation exchange capacity makes clinoptilolite rich mineral useful in waste water treatment especially in the removal of ammonium and heavy metals such as copper, cadmium, iron, lead, nickel, silver and zinc [13–30]. For the removal of anionic heavy metals such as Cr(VI) and As(V), clinoptilolite rich mineral is not as efficient as it would be in cationic heavy metals and ammonium removal. In order to improve its affinity toward Cr(VI), clinoptilolite rich mineral has been modified with acid and metal cations. Clinoptilolite rich mineral modified in this way has better removal performance than its natural form [31–35]. In recent years, bacteria species supported materials have been used as alternative material. *Arthrobacter viscosus* supported granular activated carbon and NaY, *Escherichia coli* supported granular activated carbon, kaolin and NaY zeolite are used in the Cr(VI) removal [36–41]. It has been found that the affinities of granular activated carbon, kaolin and NaY zeolite were improved by the attachment of bacteria species on the material surface. However, Cr(VI) sorption by bacteria loaded clinoptilolite rich mineral has not been subjected to study. The objective of the study is to investigate the potential application of bacteria loaded clinoptilolite rich mineral in Cr(VI) sorption.

2. Materials and methods

2.1. Sample preparation

Parent clinoptilolite rich mineral samples, from Manisa Gördes region, were grounded and classified according to different particle size ranges. After that, the samples were wet sieved to remove the soluble impurities, then dried and kept in constant relative

* Corresponding author. Tel.: +90 (232) 7506671; fax: +90 (232) 7506645.
E-mail address: beyhancansever@iyte.edu.tr (B.C. Erdoğan).

1387-1811/$ - see front matter © 2011 Elsevier Inc. All rights reserved.
doi:10.1016/j.micromeso.2011.11.002

humidity for further studies. The experiments were performed using 25–106 μm particle sized samples.

In order to prepare bacteria loaded clinoptilolite rich mineral samples, *E. coli* (NRLL-B-3008) and *Pseudomonas aeruginosa* (ATCC-27853) were chosen as gram negative bacteria. Additionally *Bacillus subtilis* (NRLL-B-4378), *Staphylococcus aureus* (ATCC-29213) and *Staphylococcus epidermidis* (ATCC-12228) were chosen as gram positive bacteria for this study. These bacteria strains were stored at −80 °C, and then grown in 8 mL Mueller Hinton Broth (Oxoid) at 37 °C for 24 h. Subsequently the cell cultures were centrifuged at 5000 rpm for 10 min. After the centrifugation, Mueller Hinton broth was removed from the cultures and the cell cultures were then suspended in 10 mL phosphate buffer solution (PBS) which was prepared by mixing 5 mM disodiumhydrogen phosphate (Na_2HPO_4) (Riedel-de Häen, 30427l), 5 mM sodiumhydrogen phosphate monohydrate ($NaH_2PO_4{\cdot}H_2O$) (Sigma S071) and 150 mM NaCl (Riedel-de Häen, 31434). PBS was vortexed by Yellowline TTS 2 for 3 s to obtain homogeneous solution. 0.1 g parent mineral samples were added into cell cultures; and the bacteria-parent mineral samples were placed in an incubator (37 °C) for 1 h. PBS solution then was refreshed to eliminate the loosely bound bacteria from the parent mineral surfaces. After that, they were placed in a thermoshaker (37 °C) for 2 h. This procedure was repeated three times under the same conditions. Finally, PBS was removed and then the samples were dried. In each step, bacteria concentrations of the samples were measured against time using Viable Cell Count method. The initial bacteria cell concentrations were determined as 1.8×10^9 CFU/mL for *E. coli*, 2.4×10^8 CFU/mL for *B. subtilis*, 1.7×10^9 CFU/mL for *S. aureus*, 1.7×10^9 CFU/mL for *S. epidermidis* and 2×10^9 CFU/mL for *P. aureginosa*.

2.2. Characterization of the samples

Identification of the crystalline species present in the parent mineral sample was established using a Philips X'Pert Pro Diffractometer (2θ = 5–80°).The purity of the sample was determined by the quantitative analysis method which has been proposed by Nakamura et al. [42]. Chemical composition of the parent mineral was estimated by Varian ICP-AES 96 Inductively Coupled Plasma Atomic Emission Spectrometer. The surface area and pore size distribution of the parent mineral was determined by Micromeritics-ASAP 2010. The parent mineral sample was dried at 150 °C for 4 h. The dried sample was degassed at 350 °C for 24 h [43]. Measurements were performed at 77 K by nitrogen as adsorptive. The functional groups on the samples were characterized by Fourier Transform IR (FTIR, Shimadzu-8201). The contribution of the electrostatic interaction between the sorbents and Cr(VI) species were determined by zeta potential (Zeta meter 3.0). Twenty milliliters of 10 mg/L Cr(VI) solution were measured at pH 5 and 6. 0.1 M NaOH and HNO_3 were used in the pH adjustment.

2.3. Batch experiments

Hexavalent chromium solution was prepared by dissolving $K_2Cr_2O_7$ (Sigma, 99.9% pure) in deionized water. 0.5 g sorbents were added into the flasks containing 10 mg/L Cr(VI) solution and then the flasks were placed in a water bath (25 °C, 140 rpm) for 4 days. Each flask was used for the estimation of the solution composition at the specified times. Samples were then taken and analyzed spectrophotometrically at λ = 540 nm using 1,5-diphenylcarbazide reagent. All sorption experiments were repeated three times. The existing Cr(VI) species in the Cr(VI) solution were estimated by pH profile studies.

The amount of Cr(VI) sorbed by sorbents and the percent of Cr(VI) removal were calculated by mass balance as follows:

$$q(t) = \frac{(C_0 - C_t)V}{m} \tag{1}$$

$$\%PR = \frac{C_0 - C_e}{C_0} \tag{2}$$

where C_0 is the initial concentration of Cr(VI) in solution (mg/L), C_t is the concentration of Cr(VI) in the solution at time t (mg/L), C_e is the concentration of Cr(VI) in the solution at equilibrium (mg/L), V is the volume of solution (L), and m is the mass of the clinoptilolite (g). Equilibrium experiments were carried out by contacting 0.5 g samples with 50 mL of Cr(VI) solution of different initial Cr(VI) concentrations 10, 50, 100, 200 and 300 mg/L. The temperature was at 25 °C.

In order to determine the reusability of the sorbents, sorption/desorption cycles were repeated five times. 0.1 M HNO_3 was used as desorption medium. 0.5 g Cr(VI) loaded samples were added into 50 mL solution containing 0.1 M HNO_3. The flasks were agitated for 120 min at a constant agitation speed of 140 rpm at 25 °C. Desorption efficiencies of the sorbents (%) were determined from the following equation:

$$\textit{Desorption efficiency} = \frac{q_{des}}{q_{sorp}} \times 100 \tag{3}$$

where q_{des} is the amount of desorbed Cr(VI) (mg/g) and q_{sorp} is the amount of sorbed Cr(VI) (mg/g).

2.4. Sorption kinetic models

Several kinetic models which are based on reaction and diffusion model are used to examine the rate of sorption process. Sorption rate covers a series of resistance resulted from diffusion and reaction steps. The diffusion of the solute across the external film surrounding the particle (external film diffusion), the diffusion of the solute in the pores (pore diffusion) and the diffusion along the sorbent surface (surface diffusion) are included in the diffusion steps. Reaction steps are involved in the sorption of the solute on the sorbent surface with surface reaction due to physical or chemical interaction. The rate limiting step is resulted from one of these step or combination of them. The experimental parameters such as agitation speed, initial concentration and temperature should be comprehensively discussed in order to decide which step should be considered as the rate limiting one.

2.4.1. Diffusion models

2.4.1.1. Mathew–Weber model. This model [44] assumes that only external film diffusion is dominant during the initial sorption period and controls the sorption process. The model equation is given in Eq. (4):

$$\ln\frac{C_t}{C_0} = -k_f S t \tag{4}$$

where C_t is the concentration of Cr(VI) ion in the solution at time t (mg/L), C_0 is the initial concentration of Cr(VI) ion in the solution (mg/L), k_f is the external mass transfer coefficient (m/s), t is the time (s), S is the surface area for mass transfer (m^{-1}):

$$S = \frac{6m/V}{d_p \rho_p (1 - \varepsilon_p)} \tag{5}$$

m is the mass of sorbent (g), V is the volume of solution (L), d_p is the particle diameter (m), ρ_p is the particle density (g/L) and ε_p is the porosity of the particle.

The initial slope of the linear plot of $\ln C_t/C_0$ versus t is used in the determination of external mass transfer coefficient (k_f).

2.4.1.2. Weber–Morris model. Weber–Morris model, which had been derived from the Fick's second law, assumes that the effect of the external mass transfer resistance is negligible, the direction of the diffusion is radial and the intraparticle diffusivity is constant [45,46]. This model was used to calculate the intraparticle diffusion rate constant. The model equation is given below:

$$q_t = k_d t^{1/2} \tag{6}$$

where q_t is the amount of Cr(VI) sorbed at time t (mg/g), k_d is the intraparticle diffusion rate constant (mg/g $min^{0.5}$) and $t^{0.5}$ is the time ($min^{0.5}$).

The intraparticle diffusion rate constant (k_d) is calculated from the slope of plot of q_t versus $t^{0.5}$. If the plot gives a straight line through the origin, intraparticle diffusion is considered as the rate limiting step. If the plot does not pass through the origin, intraparticle diffusion is not the only mechanism in the sorption process. If there are two or more mechanisms in the sorption process, the plot shows multilinearity.

2.4.2. Reaction models

2.4.2.1. Pseudo first order model. This model assumes that the rate of change of solute uptake with time is directly proportional to the difference in saturation concentration and the amount of solid uptake with time. The model equation is given below [47]:

$$\frac{dq_t}{dt} = k_1(q_e - q_t) \tag{7}$$

the integrated form of Eq. (7) becomes:

$$\log(q_e - q_t) = \log q_e - \frac{k_1}{2.303} t \tag{8}$$

where q_e and q_t are the amounts of Cr(VI) sorbed at equilibrium and at time t (mg/g), k_1 is the pseudo first order rate constant (1/min) and t is the time (min).

The pseudo first-order rate constant (k_1) is determined from the slope of the $\log(q_e - q_t)$ versus t plot.

2.4.2.2. Pseudo second order model. The pseudo second order model assumes that the sorption process is a pseudo-chemical reaction process with the driving force being the difference between the average solid concentration and the equilibrium concentration with the overall sorption rate proportional to the square of the driving force [48]. Differential form of the pseudo second-order sorption kinetic equation is expressed by Eq. (9) [49]:

$$\frac{dq_t}{dt} = k_2(q_e - q_t)^2 \tag{9}$$

where q_e and q_t are the amounts of Cr(VI) sorbed at equilibrium and at time t (mg/g), k_2 is the pseudo second-order rate constant (g mg^{-1} min^{-1}) and t is the time (min).

After integration and applying boundary conditions $t = 0$ to $t = t$ and $q_t = 0$ to $q_t = q_t$, Eq. (9) becomes:

$$\frac{1}{q_e - q_t} = \frac{1}{q_e} + k_2 t \tag{10}$$

Eq. (10) can be rearranged to obtain Eq. (11):

$$\left(\frac{t}{q_t}\right) = \frac{1}{k_2 q_e^2} + \frac{1}{q_e}(t) \tag{11}$$

Pseudo second order rate constant (k_2) is determined from the intercepts of t/q_t versus t plot.

2.5. Sorption isotherm models

2.5.1. Langmuir isotherm

Langmuir model assumes that sorption occurs at specific homogeneous sites within the adsorbents and all sites of the sorbents are identical and energetically equivalent [50]. The Langmuir model equation and its linear form are given below:

$$q_e = \frac{b q_m C_e}{1 + b C_e} \tag{12}$$

$$\frac{C_e}{q_e} = \frac{1}{q_m b} + \frac{C_e}{q_m} \tag{13}$$

where q_e and q_t are the amounts of Cr(VI) sorbed at equilibrium and at time t (mg/g), q_m is maximum sorption capacity (mg/g) and b is Langmuir constant (L/mg).

Maximum sorption capacity and the Langmuir constant are estimated from slope and intercept of the C_e/q_e versus C_e plot, respectively.

2.5.2. Freundlich isotherm

Freundlich isotherm, which is the earliest known relationship, describes the non-ideal and reversible adsorption [51]. The model equation and its linear form are written as:

$$q_e = k_F \cdot C_e^{1/n} \tag{14}$$

$$\log q_e = \log k_F + \frac{1}{n} \log C_e \tag{15}$$

where q_e and q_t are the amount of Cr(VI) sorbed at equilibrium and at time t (mg/g), k_F is the Freundlich constant and $1/n$ is the heterogeneity factor.

The slope and intercept of the linear plot of $\log q_e$ versus $\log C_e$ are used to determine heterogeneity factor ($1/n$) and Freundlich constant (k_F), respectively.

2.5.3. Dubinin–Radushkevich isotherm

Dubinin–Radushkevich (DR) isotherm model is based on the assumption that the characteristics of sorption curves relate to the porous structure of the sorbent [52]. The model equation and its linear form are given below:

$$q_e = q_m \exp(-K\varepsilon^2) \tag{16}$$

$$\ln q_e = \ln q_m - K\varepsilon^2 \tag{17}$$

$$\varepsilon = RT\left(1 + \frac{1}{C_e}\right) \tag{18}$$

where ε is Polanyi potential, R is the gas constant (8.314×10^{-3} kJ/mol K) and T is the temperature (K), C_e is the equilibrium concentration (mg/L), q_m is the maximum adsorption capacity based on D–R isotherm (mg/g) and K is the constant related to the sorption energy (mol^2/kJ^2).

The slope and intercept of the linear plot of $\ln q_e$ versus ε^2 are used to determine sorption energy constant (K) and maximum adsorption capacity based on D–R isotherm (q_m), respectively.

The mean adsorption energy (E) is calculated from the following equation:

$$E = \frac{1}{\sqrt{2K}} \tag{19}$$

where E is the mean adsorption energy (kJ/mol) and K is the constant related to the sorption energy (mol^2/kJ^2).

The magnitude of the mean adsorption energy gives an idea about the type of sorption whether it is physical or chemical. If

its value is lower than 8 kJ/mol, sorption is physically controlled. If the value is between 8 and 16 kJ/mol, sorption is controlled by chemical sorption.

3. Results and discussion

3.1. pH profiles of sorbents in Cr(VI) solution

The form of Cr(VI) species existing in the medium should also be considered in the explanation of the sorption mechanism. Cr(VI) can be found in the forms of H_2CrO_4, $HCrO_4^-$, CrO_4^{-2}, $Cr_2O_7^{-2}$ and $HCr_2O_7^-$ depending on the pH and the total Cr(VI) concentration in the solution. As it is seen from the Fig. 1, Cr(VI) is mainly found as $HCrO_4^-$ in the pH range of 1–5; while in the pH range of 8–14 it exists in the form of CrO_4^-2.However both forms exist in the pH range between 6 and 7.

pH profiles of the parent mineral and bacteria loaded samples in Cr(VI) solutions (Fig. 2) were in the range of 5.1–5.9, which has implied the existence of only $HCrO_4^-$ and CrO_4^-2 forms of the Cr(VI) in the solution and interactions of them with the sorbents.

3.2. Effect of experimental parameters on Cr(VI) sorption

3.2.1. Effect of initial concentration

The experimental studies were carried out with varying initial metal ion concentrations of Cr(VI) ranging from 10 to 300 mg/L, at 25 °C and 140 rpm. The effect of initial concentration on sorption of Cr(VI) by *E. coli* loaded clinoptilolite rich mineral is shown in Fig. 3. The trend for each sorbents was observed to be similar. As shown in these figures, uptake rate of Cr(VI) was rapid at the beginning of the sorption process due to the availability of large number of unoccupied sites in the sorbent. As sorption time progressed, Cr(VI) uptake rate gradually slowed down since the sites in the sorbents were occupied and fewer available sites were involved in the sorption process. The results also indicated that at equilibrium the amount of Cr(VI) sorbed by the sorbent increased with increasing initial concentration.

Cr(VI) removal percentage values of all the sorbents at two different initial concentrations are tabulated in Table 1. As indicated in Table 1, Cr(VI) removal percentage value of the parent mineral was slightly increased after the attachment of bacteria to its surface. The results also indicated that Cr(VI) removal with gram positive bacteria loaded parent mineral samples were slightly higher than gram negative bacteria loaded samples. This is explained by the nature of the cell wall constituents. Secondary polymers which only present on the gram positive cell wall structure enhanced the interaction between Cr(VI) species and the sorbents and thus higher Cr(VI) sorption values were observed with gram positive bacteria loaded parent mineral samples.

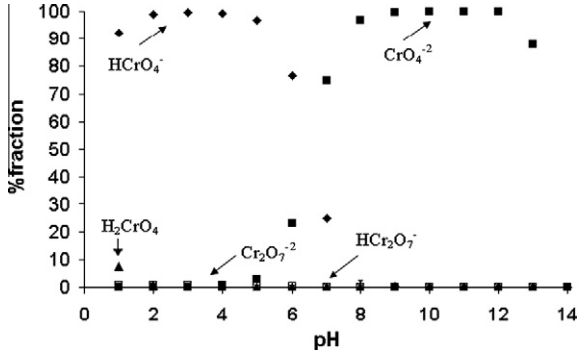

Fig. 1. Cr(VI) speciation diagram.

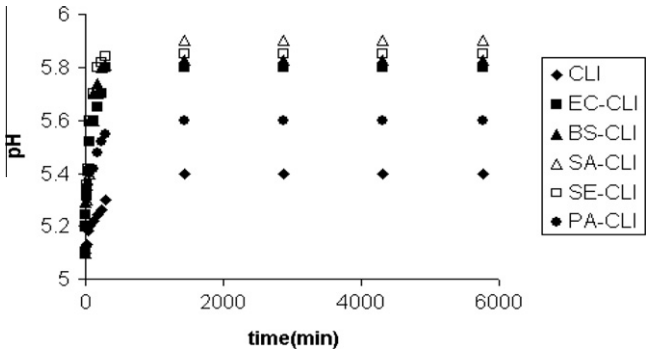

Fig. 2. pH profiles of the parent mineral and bacteria loaded forms in Cr(VI) solution.

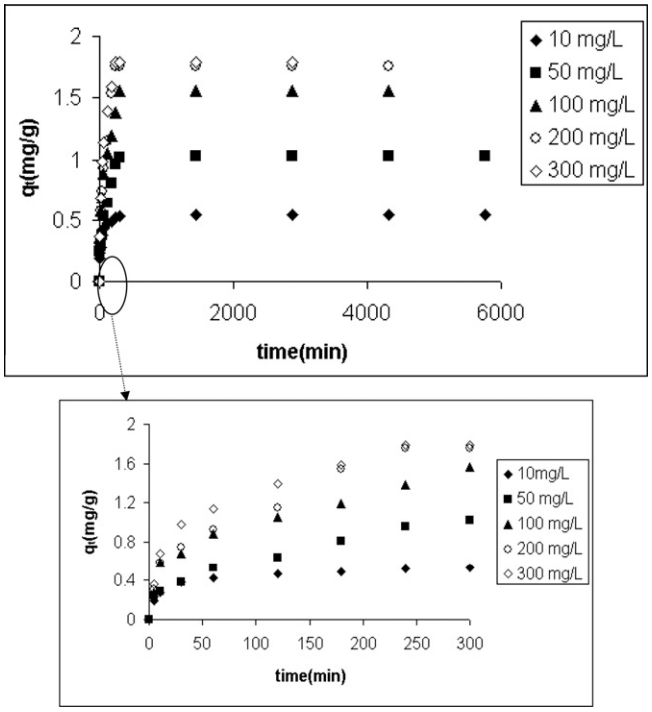

Fig. 3. Effect of initial concentration on the sorption of Cr(VI) by *E. coli* loaded clinoptilolite rich mineral (temperature: 25 °C, agitation speed: 140 rpm, particle size: 25–106 μm).

Table 1
Cr(VI) removal percentage values of all sorbents at different initial concentrations.

Sorbents	% Cr(VI) removal	
	10 mg/L	300 mg/L
Clinoptilolite rich mineral	48	4.6
E. coli loaded clinoptilolite rich mineral	54	5.9
B. subtilis loaded clinoptilolite rich mineral	58	9.1
S. aureus loaded clinoptilolite rich mineral	56	6.4
S. epidermidis loaded clinoptilolite rich mineral	55	6.3
P. aeuriginosa loaded clinoptilolite rich mineral	50	5.0

3.2.2. Effect of agitation speed

The effect of agitation speed on Cr(VI) sorption by *E. coli* loaded clinoptilolite rich mineral at different stirring speeds, ranging from 60 to 140 rpm, is shown in Fig. 4. Similar results were obtained with clinoptilolite and *B. subtilis*, *S. aureus*, *S. epidermidis* and *P. aeruginosa* loaded clinoptilolite rich mineral. It is well known that the formation of the external film boundary layer is influenced by

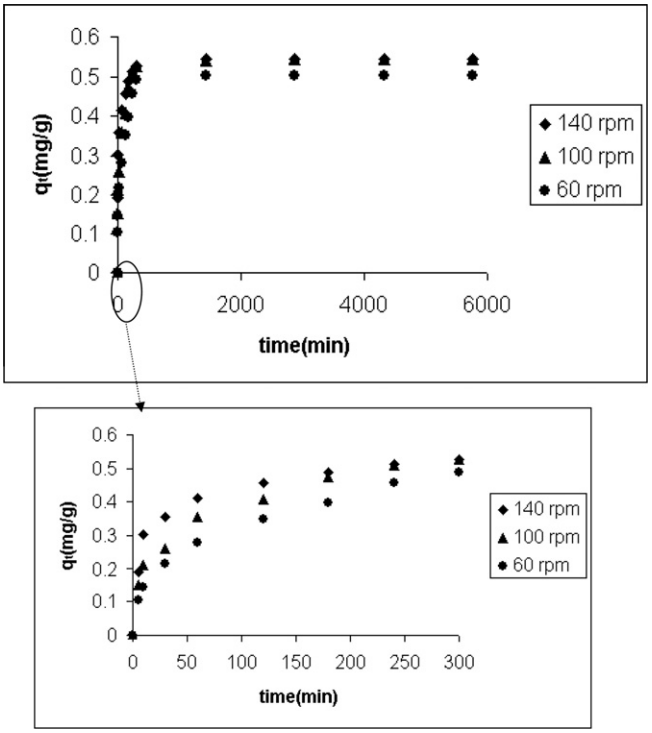

Fig. 4. Effect of agitation speed on the sorption of Cr(VI) by *E. coli* loaded clinoptilolite rich mineral (concentration: 10 mg/L, temperature: 25 °C, particle size: 25–106 μm).

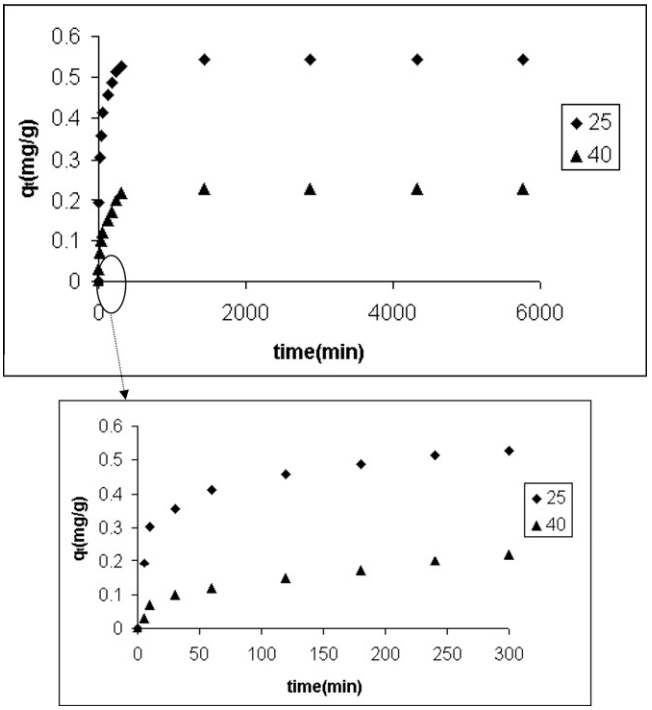

Fig. 5. Effect of temperature on the sorption of Cr(VI) by *E. coli* loaded clinoptilolite rich mineral (concentration: 10 mg/L, agitation speed: 140 rpm, particle size: 25–106 μm).

the agitation speed. By increasing the agitation speed, the thickness of the boundary layer decreases and thus the external mass resistance becomes smaller. As seen in the figures, initial uptake rate increased with increasing agitation speed. The results also showed that at equilibrium the amount of Cr(VI) sorbed by the sorbent was independent of the agitation speed.

3.2.3. Effect of temperature

The effect of temperature on the Cr(VI) sorption by *E. coli* loaded clinoptilolite rich mineral is shown in Fig. 5. The results indicated that the amount of Cr(VI) sorbed at equilibrium, and the initial uptake rate were decreased when the temperature was increased from 40 to 25 °C. Similar trend was observed with the parent mineral and *B. subtilis*, *S. aureus*, *S. epidermidis* and *P. aeruginosa* loaded parent mineral. The decrease in Cr(VI) sorption with increasing temperature indicated the weak interaction between sorbents and Cr(VI) species and this supported physical sorption. Moreover, the decrease in sorption with increasing temperature showed exothermic nature of the Cr(VI) sorption process.

3.3. Sorption kinetic model results

External mass transfer coefficient (k_f), intraparticle diffusion rate constant (k_d), pseudo first (k_1) and second order (k_2) rate constant were determined for the experimental parameters including initial concentration, agitation speed and temperature. Their values are tabulated in Tables 2–7. As seen from the tables, the effects of initial concentration, agitation speed and temperature are similar for all the sorbents (clinoptilolite rich mineral and bacteria loaded forms). The correlation coefficients of Mathew–Weber model were in the range of 0.87–0.97. The correlation coefficient (R^2) values of Weber–Morris model were higher than 0.94. For the pseudo first order kinetic model, the obtained R^2 values were between 0.78 and 0.98. The values of R^2 for the pseudo second-order model were always greater than 0.99. The results indicated that pseudo-second order kinetic model and Weber–Morris model fitted well with the experimental data better than the pseudo first order kinetic model and Mathew–Weber model. Similar results were obtained with the parent mineral and bacteria loaded forms.

The validity of the sorption kinetic models was also checked by the comparison of the experimental and theoretical model results. Using the external mass transfer coefficient obtained from Mathew and Weber Model, the comparison of the theoretical and experimental decay curves for *E. coli* loaded clinoptilolite rich mineral is shown in Fig. 6. The results indicated that the experimental and theoretical data were closer during the first 10 min of the sorption period. After approximately 10 min, the deviation between experimental and theoretical results showed the effectiveness of the other mass transfer resistances. Fig. 7 shows the comparison of theoretical and experimental results of Weber–Morris model. The results indicated that the experimental and theoretical data were closer after 10 min. The deviation during 10 min implied that the external mass transfer was much more effective in the sorption process during this period. After that, intraparticle diffusion governed the sorption process. Fig. 8 shows the comparison of the experimental and reaction model results. As it is seen from the figure that, pseudo second order model was fitted well to experimental data.

3.4. Characterization studies

XRD characteristic peaks of the parent mineral were observed at $2\theta = 9.76°$, 22.23° and 30.05° and the purity of the sample was found to be 90%. Chemical composition of the parent mineral was: 65.1% SiO_2, 12.6% Al_2O_3, 1.42% Fe_2O_3, 3.93% K_2O, 0.92% Na_2O, 1.92% CaO, 0.85% MgO and 13.4% H_2O. BET surface area for parent mineral was found as 49.5 m^2/g and the pore size distribution of it is given in Fig. 9. The results indicated that pore sizes

Table 2
The values of model constants at different conditions for clinoptilolite rich mineral.

Parameters		MW[a] $k_f \times 10^6$ (m/min)	WM $k_d \times 10^3$ (mg/g min$^{0.5}$)	PFO $k_1 \times 10^3$ (min^{-1})	PSO $k_2 \times 10^3$ (g/mg min)
Initial concentration (mg/L)	10	15.6	26.9	21.7	51.9
	50	7.3	29.7	20.5	40.7
	100	4.8	45.8	19.8	37.8
	200	1.9	70.1	17.7	32.5
	300	1.5	72.8	14.1	23.8
Agitation speed (rpm)	60	10.1	21.7	8.9	20.8
	100	12.8	23.1	11.2	34.8
	140	15.6	26.9	21.7	51.9
Temperature (°C)	25	15.6	26.9	21.7	51.9
	40	7.6	11.3	16.1	15.5

[a] MW: Mathew–Weber, WM: Weber–Morris, PFO: pseudo-first order model, PSO: pseudo-second order model.

Table 3
The values of model constants at different conditions for *E. coli* loaded clinoptilolite rich mineral.

Parameters		MW[a] $k_f \times 10^6$ (m/min)	WM $k_d \times 10^3$ (mg/g min$^{0.5}$)	PFO $k_1 \times 10^3$ (min^{-1})	PSO $k_2 \times 10^3$ (g/mg min)
Initial concentration (mg/L)	10	42	30.4	37	160
	50	7.6	51.4	24.8	30.5
	100	5.1	62.6	17.2	27.5
	200	3.7	77	16.3	20.6
	300	2.9	96.5	12.7	19.7
Agitation speed (rpm)	60	16.1	19.5	18.7	55.2
	100	26.7	23.6	22.4	64.9
	140	42	30.4	37	160
Temperature (°C)	25	42	30.4	37	160
	40	9.2	9.7	17.9	110.4

[a] MW: Mathew–Weber, WM: Weber–Morris, PFO: pseudo-first order model, PSO: pseudo-second order model.

Table 4
The values of model constants at different conditions for *B. subtilis* loaded clinoptilolite rich mineral.

Parameters		MW[a] $k_f \times 10^6$ (m/min)	WM $k_d \times 10^3$ (mg/g min$^{0.5}$)	PFO $k_1 \times 10^3$ (min^{-1})	PSO $k_2 \times 10^3$ (g/mg min)
Initial concentration (mg/L)	10	46.6	25.2	30.2	116.1
	50	12.9	51.4	21.4	24.2
	100	7.6	62.6	19.1	19.4
	200	5.1	74.6	16.3	11.3
	300	4.2	101	13.8	10.8
Agitation speed (rpm)	60	16.1	19.5	14.9	44.4
	100	31.1	21.2	23.5	67.6
	140	46.6	25.2	30.2	116.1
Temperature (°C)	25	46.6	25.2	30.2	116.1
	40	6.4	12.1	13.2	75.9

[a] MW: Mathew–Weber, WM: Weber–Morris, PFO: pseudo-first order model, PSO: pseudo-second order model.

distribution of the sample was in the range of 25–110 Å. Regarding the pore size distribution, the sample has a mesoporous structure.

In order to asses the contributions of the non-electrostatic forces in the sorption mechanism, further characterizations studies were performed by FTIR. The FTIR result of the parent mineral after Cr(VI) sorption is given in Fig. 10. Characteristic bands of the clinoptilolite related to T–O streching, T–O bending, OH streching, hydrogen bonding of water and water bending were observed at 1085, 476, 3672, 3477 and 1672 cm^{-1}, respectively. Band shift in the water molecules, which was an indication of existence of hydrogen bonding, was observed after Cr(VI) sorption. Similar FTIR results were observed with bacteria loaded samples.

In order to understand the contribution from electrostatic interaction between sorbents and Cr(VI) species, zeta potentials of the sorbents in Cr(VI) solution at pH 5 and 6 had to be measured. Average values are tabulated in Table 8. The results implied that the surfaces of the parent mineral and bacteria loaded samples were negatively charged; and thus repulsive electrostatic forces could exist between the sorbents and anionic Cr(VI) species. Although there were repulsive electrostatic forces, Cr(VI) sorption was observed and these results indicate the contribution of the non-electrostatic forces in connection with hydrogen bonding. The existence of hydrogen bonding was confirmed by the band shift in the FTIR results.

3.5. Sorption isotherm model results

Equilibrium data of the experimental results were fitted to Langmuir, Freundlich and D–R model isotherms. Values of the model constants are tabulated in Table 9. The correlation coeffi-

Table 5
The values of model constants at different conditions for *S. aureus* loaded clinoptilolite rich mineral.

Parameters		MW[a] $k_f \times 10^6$ (m/min)	WM $k_d \times 10^3$ (mg/g min$^{0.5}$)	PFO $k_1 \times 10^3$ (min^{-1})	PSO $k_2 \times 10^3$ (g/mg min)
Initial concentration (mg/L)	10	43.1	29.0	37.3	147.3
	50	13.0	48.7	22.8	32.6
	100	8.8	60.3	21.2	23.2
	200	3.7	77.1	17.9	20.6
	300	2.9	96.5	16.4	19.4
Agitation speed (rpm)	60	14.7	20.6	13.8	61.5
	100	26.5	24.6	19.4	78.7
	140	43.1	29.0	37.3	147.3
Temperature (°C)	25	43.1	29.0	37.3	147.3
	40	10.3	11.8	14.1	77.8

[a] MW: Mathew–Weber, WM: Weber–Morris, PFO: pseudo-first order model, PSO: pseudo-second order model.

Table 6
The values of model constants at different conditions for *S. epidermidis* loaded clinoptilolite rich mineral.

Parameters		MW[a] $k_f \times 10^6$ (m/min)	WM $k_d \times 10^3$ (mg/g min$^{0.5}$)	PFO $k_1 \times 10^3$ (min^{-1})	PSO $k_2 \times 10^3$ (g/mg min)
Initial concentration (mg/L)	10	48.6	27.5	36.7	153.8
	50	15.5	47.6	22.1	28.1
	100	9.4	61.5	20.7	25.6
	200	3.8	77.2	19.3	22.4
	300	3.5	96.1	15.9	20.1
Agitation speed (rpm)	60	21.9	18.2	17.5	54.5
	100	34.5	20.6	27.1	115.2
	140	48.6	27.5	36.7	153.8
Temperature (°C)	25	48.6	27.5	36.7	153.8
	40	7.8	12.0	13.8	120.2

[a] MW: Mathew–Weber, WM: Weber–Morris, PFO: pseudo-first order model, PSO: pseudo-second order model.

Table 7
The values of model constants at different conditions for *P. aeuriginosa* loaded clinoptilolite rich mineral.

Parameters		MW[a] $k_f \times 10^6$ (m/min)	WM $k_d \times 10^3$ (mg/g min$^{0.5}$)	PFO $k_1 \times 10^3$ (min^{-1})	PSO $k_2 \times 10^3$ (g/mg min)
Initial concentration (mg/L)	10	24.9	29.9	26.2	84.6
	50	9.9	44.3	19.5	32.1
	100	6.2	47.6	17.3	24.1
	200	2.4	70.8	16.1	21.9
	300	1.6	71.1	15.2	19.9
Agitation speed (rpm)	60	16.1	21.1	15.9	39.8
	100	20.6	24.8	16.8	54.9
	140	24.9	29.9	26.2	84.6
Temperature (°C)	25	24.9	29.9	26.2	84.6
	40	9.2	11.6	17.8	29.1

[a] MW: Mathew–Weber, WM: Weber–Morris, PFO: pseudo-first order model, PSO: pseudo-second order model.

cients (R^2) of Langmuir model were higher than 0.99 whereas the correlation coefficients of Freundlich and D–R isotherm models were lower than 0.98 and 0.87, respectively. Higher correlation coefficients indicate better representation by the Langmuir isotherm model. Equilibrium isotherm data for Cr(VI) sorption with *E. coli* loaded clinoptilolite rich mineral is given in Fig. 11. As it is seen from the figures, equilibrium data was very well represented by the Langmuir isotherm model. Similar results were obtained with the parent mineral and bacteria loaded forms.

3.6. Reusability of the sorbents

Table 10 shows the results of sorption–desorption cycles for *E. coli* loaded clinoptilolite rich mineral. The results indicated that the desorption efficiency was above 81% when the sorbent was reused after five times. Desorption efficiency trend for each sorbents was observed to be similar. Based on the economic point of view; the usage of parent mineral and bacteria loaded forms in Cr(VI) removal was feasible.

4. Conclusion

The performances of the parent mineral and bacteria loaded samples in Cr(VI) sorption were established. The results implied that functional groups on the bacteria species enhanced the interaction between Cr(VI) species and bacteria loaded samples and thus higher Cr(VI) sorption values were observed with the bacteria loaded samples. When Cr(VI) sorption performances of the bacteria loaded samples were compared, Cr(VI) sorption with the gram positive bacteria loaded samples were slightly higher than the gram negative bacteria loaded samples. The reason was explained by the difference between cell wall structures. Secondary polymers

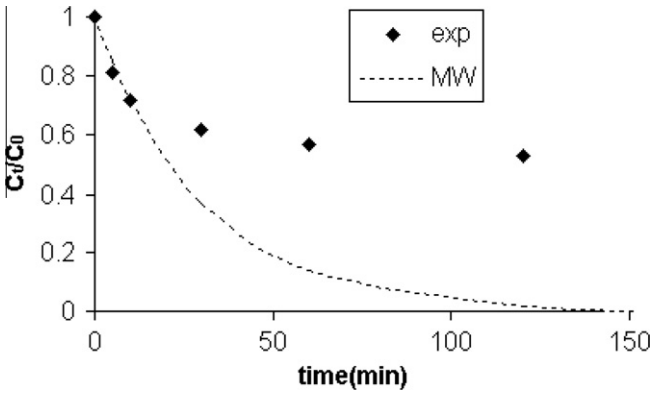

Fig. 6. Comparison of theoretical and experimental concentration decay curve for the *E. coli* loaded clinoptilolite rich mineral (concentration: 10 mg/L, agitation speed: 140 rpm, particle size: 25–106 μm, temperature: 25 °C).

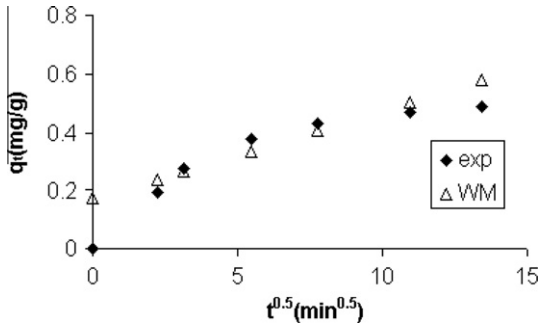

Fig. 7. Comparison of theoretical and experimental Weber–Morris model results for the *E. coli* loaded clinoptilolite rich mineral (concentration: 10 mg/L, agitation speed: 140 rpm, particle size: 25–106 μm, temperature: 25 °C).

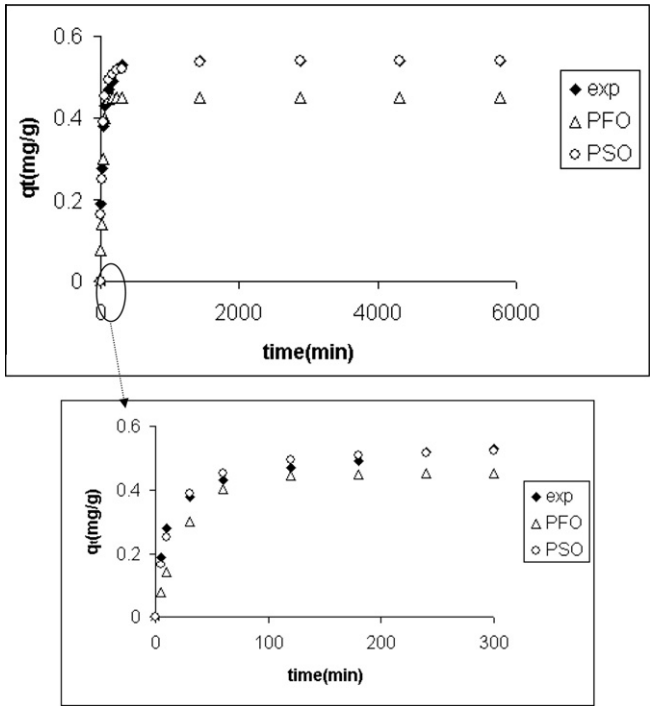

Fig. 8. Comparison of the experimental and reaction model results for *E.Coli* loaded clinoptilolite rich mineral (concentration: 10 mg/L, agitation speed: 140 rpm, particle size: 25–106 μm, temperature: 25 °C).

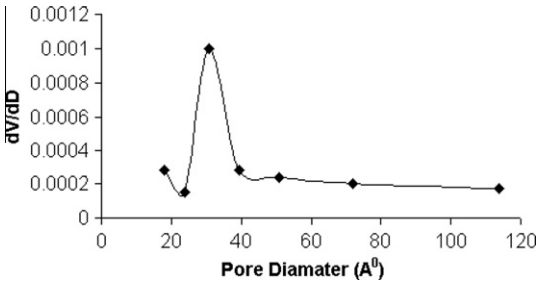

Fig. 9. Pore size distribution of the parent mineral.

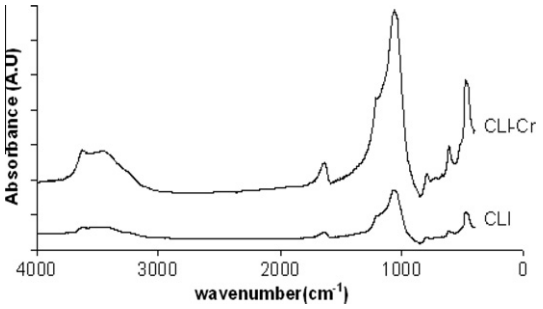

Fig. 10. FTIR results of parent mineral and after Cr(VI) sorption.

Table 8
Average zeta potential values of sorbents in 10 mg/L Cr(VI) solution at pH 5 and 6 (five measurement).

Samples	pH 5 Zeta potential (mV)	pH 6 Zeta potential (mV)
Clinoptilolite rich mineral	−28.9	−31.9
E.coli loaded clinoptilolite rich mineral	−32.4	−33.4
B. subtilis loaded clinoptilolite rich mineral	−31.9	−32.8
S. aureus loaded clinoptilolite rich mineral	−28.4	−29.2
S. epidermidis loaded clinoptilolite rich mineral	−27.2	−28.6
P. aeuriginosa loaded clinoptilolite rich mineral	−29.4	−30.6

Table 9
Isotherm model parameters.

Sorbents	Langmuir			Freundlich			D–R		
	q_m	b	R^2	k_f	n	R^2	q_m	K	R^2
CLI	1.52	0.03	0.987	0.3	3.64	0.978	9.9	0.35	0.786
EC-CLI	1.93	0.046	0.995	0.34	3.24	0.967	15.8	0.37	0.868
BS-CLI	2.44	0.045	0.996	0.39	3.0	0.975	21.3	0.38	0.937
SA-CLI	2.02	0.051	0.997	0.37	3.26	0.968	17.8	0.38	0.939
SE-CLI	1.99	0.065	0.999	0.39	3.29	0.953	17.6	0.38	0.951
PA-CLI	1.49	0.058	0.998	0.34	3.77	0.977	11.7	0.36	0.931

which only present on the gram positive cell wall structure enhanced the interaction between the Cr(VI) species and the sorbents. Thus higher Cr(VI) was obtained with the gram positive bacteria loaded samples.

Zeta potential results of the samples imply the existence of repulsive forces between the parent mineral and the Cr(VI) species, and between the bacteria loaded samples and the Cr(VI) species. Although there were repulsive electrostatic forces, the existence

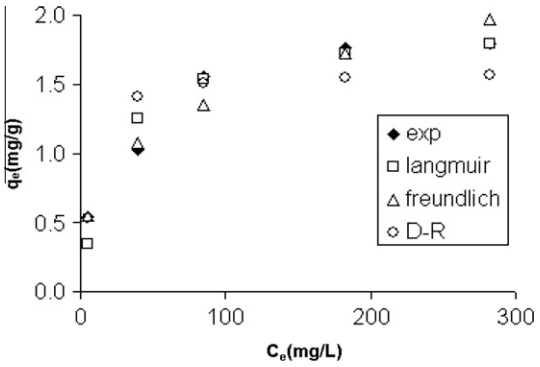

Fig. 11. Equilibrium isotherm for Cr(VI) sorption by *E. coli* loaded clinoptilolite rich mineral at 25 °C.

Table 10
Sorption–desorption cycles for *E. coli* loaded clinoptilolite rich.

	Sorption–desorption cycle				
	1	2	3	4	5
Sorption amount (mg/g)	0.54	0.51	0.48	0.45	0.43
Desorption amount (mg/g)	0.50	0.46	0.42	0.37	0.35
Desorption Efficiency (%)	92	90	88	82	81

of Cr(VI) sorption indicates a significant role of the non-electrostatic forces in Cr(VI) sorption.

Sorption diffusion model results implied that external and intraparticle diffusion are effective in Cr(VI) sorption; external film diffusion was effective at the beginning of the sorption process; thereafter, it is tended to be controlled by the intraparticle diffusion. Sorption reaction model results showed that the Cr(VI) sorption fitted well to pseudo second order model. Sorption isotherm results indicated that the experimental data is represented very well by Langmuir isotherm model

As a summary, gram positive bacteria loaded parent mineral samples are promising materials in Cr(VI) removal.

Acknowledgements

The authors are grateful to Turkish Republic Prime Ministry State Planning Organization (DPT-1998 K122130) for financial support. The authors thank to Dr. Hürriyet Polat for zeta potential analysis. The authors also thank to Dr. Ayben Top for her valuable discussion and contribution.

References

[1] J. Kotas, Z. Stasicka, Environ. Pollut. 107 (2000) 263–283.
[2] A. Leonard, R.R. Lauwerys, Mutat. Res. 76 (1980) 227–239.
[3] C. Pellerin, S.M. Booker, Environ. Health Perspect. 108 (2000) 402–407.
[4] F.A. Mumpton, PNAS 96 (1999) 3463–3470.
[5] G.A. Armenta, M.E.P. Iglesias, R.L. Ramos, Adsorpt. Sci. Technol. 21 (2003) 81–91.
[6] M.W. Ackley, S.U. Rege, H. Saxena, Micropor. Mesopor. Mater. 61 (2003) 25–42.
[7] F.C. Özkan, S. Ülkü, Micropor. Mesopor. Mater. 77 (2005) 47–53.
[8] H. Faghihian, M. Talebi, M. Pirouzi, J. Iran. Chem. Soc. 5 (2008) 394–399.
[9] K. Pavelic, M. Hadzija, L. Bedrica, J. Pavelic, I. Dikic, M. Katic, M. Kralj, M.H. Bosnar, S. Kapitanovic, M. Poljak-Blazi, S. Krizanac, R. Stojkovic, M. Jurin, B. Subotic, M. Colic, J. Mol. Med. 78 (2001) 708–720.
[10] K. Pavelic, M. Katic, V. Sverko, T. Marotti, B. Bosnjak, T. Balog, R. Stojkovic, M. Radacic, M. Colic, M. Poljak-Blazi, J. Cancer Res. Clin. 128 (2002) 37–44.
[11] S. Göktaş, S. Ülkü, O. Bayraktar, Appl. Clay Sci. 40 (2008) 6–14.
[12] G. Narin, Ç.B. Albayrak, S. Ülkü, Appl. Clay Sci. 50 (2010) 560–568.
[13] S. Ülkü, Application of Natural Zeolites in Water Treatment, Çevre '84-Umwelli '84; V. Deutch- Turkisches Symposium fur Unweltingenieurwesen, 1984.
[14] A.E. Şenatalar, A. Sirkecioğlu, Turkish J. Eng. Env. Sci. 19 (1995) 399–405.
[15] A. Langella, M. Pansini, P. Cappelletti, B. de Gennaro, M. de' Gennaro, C. Colella, Micropor. Mesopor. Mater. 37 (2000) 337–343.
[16] R. Petrus, J. Warchol, Micropor. Mesopor. Mater. 61 (2003) 137–146.
[17] A.S. Sheta, A.M. Falatah, M.S. Al-Sewailem, E.M. Khaled, A.S.H. Sallam, Micropor. Mesopor. Mater. 61 (2003) 127–136.
[18] A. Top, S. Ülkü, Appl. Clay Sci. 27 (2004) 13–19.
[19] D. Karadağ, Y. Koç, M. Turan, B. Armağan, J. Hazard. Mater. 136 (2006) 604–609.
[20] M. Akgül, A. Karabakan, O. Acar, Y. Yürüm, Micropor. Mesopor. Mater. 94 (2006) 99–104.
[21] A. Günay, E. Arslankaya, İ. Tosun, J. Hazard. Mater. 146 (2007) 362–371.
[22] M.E. Argün, J. Hazard. Mater. 150 (2008) 587–595.
[23] N.A. Öztas, A. Karabakan, Ö. Topal, Micropor. Mesopor. Mater. 111 (2008) 200–205.
[24] P. Vassileva, D. Voikova, J. Hazard. Mater. 170 (2009) 948–953.
[25] N. Karapınar, J. Hazard. Mater. 170 (2009) 1186–1191.
[26] T. Motsi, N.A. Rowson, M.J.H. Simmons, Int. J. Miner. Process. 92 (2009) 42–48.
[27] A. García-Mendieta, M. Solache-Ríos, M.T. Olguín, Micropor. Mesopor. Mater. 118 (2009) 489–495.
[28] H. Huang, X. Xiao, B. Yan, L. Yang, J. Hazard. Mater. 175 (2010) 247–252.
[29] N. Lihareva, L. Dimova, O. Petrov, Y. Tzvetanova, Micropor. Mesopor. Mater. 130 (2010) 32–37.
[30] Ö. Can, D. Balköse, S. Ülkü, Desalination 259 (2010) 17–21.
[31] R. Toprak, İ. Girgin, Turkish J. Eng. Env. Sci. 24 (2000) 343–351.
[32] M.C. Mier, R.L. Callejas, R. Gehr, B.J. Cisneros, P.J. Alvares, Water Res. 35 (2001) 373–378.
[33] S. Babel, T.A. Kurniawan, Ion Ex. 14 (2003) 289–292.
[34] H. Faghihian, R. Bowman, Water Res. 39 (2005) 1099–1104.
[35] Y. Orhan, S. Kocaoba, Anal. Chim. 97 (2007) 781–790.
[36] C. Quintelas, B. Fernandes, J. Castro, H. Figueiredo, T. Tavares, J. Hazard. Mater. 153 (2008) 799–809.
[37] S. Lameiras, C. Quintelas, T. Tavares, Bioresour. Technol. 99 (2008) 801–806.
[38] B. Silva, H. Figueiredo, C. Quintelas, I.C. Neves, T. Tavares, Micropor. Mesopor. Mater. 116 (2008) 555–560.
[39] C. Quintelas, Z. Rocha, B. Silva, B. Fonseca, H. Figueiredo, T. Tavares, Chem. Eng. J. 149 (2009) 319–324.
[40] C. Quintelas, Z. Rocha, B. Silva, B. Fonseca, H. Figueiredo, T. Tavares, Chem. Eng. J. 152 (2009) 110–115.
[41] R.M. Gabr, S.M.F. Gad El-Rab, R.N.N. Abskharon, S.H.A. Hassan, A.A.M. Shoreit, World J. Microbiol.Biotechnol. 25 (2009) 1695–1703.
[42] T. Nakamura, M. Ishikawa, T. Hiraiwa, J. Sato, Anal. Sci. 8 (1992) 539–543.
[43] Y. Akdeniz, S. Ülkü, J. Porous Mat. 14 (2007) 55–60.
[44] A.P. Mathews, W.J. Weber, AIChE J. 73 (1976) 91–107.
[45] J. Weber, J.C. Morris, J. Sanit, Eng. Div. ASCE 89 (1963) 31–59.
[46] G.F. Malash, M.I. El-Khaiary, Chem. Eng. J. 163 (2010) 256–263.
[47] S. Lagergren, K. Svensk, Vet. Akad. Handl. 24 (1898) 1–39.
[48] X. Yang, B. Al-Duri, J. Colloid Interf. Sci. 287 (2005) 25–34.
[49] Y.S. Ho, J.C.Y. Ng, G. McKay, Separ. Purif. Method 29 (2000) 189–232.
[50] I. Langmuir, J. Am. Chem. Soc. 40 (1918) 1361–1403.
[51] H. Freundlich, Z. Phys. Chem. 57 (1906) 384–410.
[52] M.M. Dubinin, L.V. Radushkevich, Proc. Acad. Sci. Phys. Chem. Sect. 55 (1947) 331–333.